Journal of Materials Chemistry C

ROYAL SOCIETY OF CHEMISTRY

PAPER

View Article Online
View Journal | View Issue

Check for updates

Cite this: J. Mater. Chem. C, 2022, 10, 2648

Published on 09 november 2021. Downloaded on 2025-01-07 13:39:47.

Highly sensitive solid chemical sensor for veterinary drugs based on the synergism between hydrogen bonds and low-dimensional polymer networks†

Junhua Kuang,[ab] Jie Yang,[c] Kai Liu,[ab] Zhiyuan Zhao,[a] Wei Shi,[a] Mingchao Shao,[ab] Yangshuang Bian,[ab] Yanwei Liu,[ab] Jinyang Chen,[ab] Mingcong Qin,[ab] Lang Jiang,[a] Jichen Dong,[a] Yunlong Guo *[a] and Yunqi Liu[a]

Received 31st August 2021,
Accepted 8th November 2021

DOI: 10.1039/d1tc04114b

rsc.li/materials-c

The safety of animal-origin foods has a major influence on human health. Although the use of veterinary drug additives (VDAs) significantly promotes the normal growth and development of animals against diseases, the excessive consumption of VDAs is always the most worrying part. Thus, realizing a direct and prompt detection of solid VDAs is highly desirable. In this study, we incorporated a functional unit of triazolo [4,5-*c*] pyridine (TP) in polymer semiconductors. The theoretical simulation demonstrates that TP can effectively form hydrogen bonding with the VDA molecules. Furthermore, highly sensitive polymeric field-effect transistors (PFETs) are fabricated through the configurational design of low-dimensional polymer networks (LDPNs). The conducting channel and hydrogen bonding sites of the LDPN-based PFETs could be directly exposed to the analytes, thereby effectively capturing VDA molecules and converting the stimuli into electrical signals. The obtained PFET-based solid sensors showed highly sensitive and stable detection of melamine powders at a low operation voltage of −5 V. The detection limit realized is lower than the international standards in animal feeds (2.5 ppm). These results demonstrate the promising applications of PFETs for high-efficiency and low-power-consumption sensors for solid detection or biological diagnosis.

Introduction

The safety of animal-origin foods has garnered considerable attention due to the ineluctable residues of veterinary drug additives (VDAs). Although the use of VDAs in animal feeds is beneficial to prevent and cure animal diseases, and improve food production, the excessive consumption of VDAs is the most worrying part of this process, as it will cause severe damage to human beings.[1] However, most of the existing analytical instruments require expensive equipment and entail complex sample-preparation processes to qualify and quantify VDAs.[2] To overcome this challenge, there is an urgent requirement to develop brand-new methodologies to achieve rapid, effective and direct detection of solid VDAs.

Organic field-effect transistors (OFETs) have shown great potential for enabling highly sensitive sensing applications owing to their signal conversion and amplification.[3–6] OFET-sensors are widely employed to detect chemical vapors,[7–15] pressure[16–19] and photons,[20–26] as well as chemicals in liquid environments.[27,28] However, currently very few reports involve research on the detection of solid analytes.[29,30] Therefore, it remains a considerable challenge to achieve the effective detection of solid powders. This is primarily because the required high semiconductor film thickness (>30 nm) for high-mobility OFETs severely restricts the diffusion of analyte molecules across the active layer and degrades the interaction between analytes and semiconductors.[30] Therefore, reducing the semiconductor film thickness and improving the interaction between analytes and semiconductors are two efficient strategies to realize rapid detection of VDAs. In addition, polymeric FETs (PFETs) are one of the most promising devices in the design of low-cost and sensitive solid sensors, due to polymer semiconductors possessing designable molecular skeletons, excellent film-forming properties, and low-cost solution processability.[31–37]

In this study, we propose a highly sensitive PFET based on a polymer structure with the designed adsorption sites and

[a] Beijing National Laboratory for Molecular Sciences, CAS Key Laboratory of Organic Solids, Institute of Chemistry, Chinese Academy of Sciences, Beijing 100190, China. E-mail: guoyunlong@iccas.ac.cn
[b] University of Chinese Academy of Sciences, Beijing 100049, China
[c] Department of Materials Science and Engineering, City University of Hong Kong, Kowloon, Hong Kong SAR 999077, China

† Electronic supplementary information (ESI) available. See DOI: 10.1039/d1tc04114b

This journal is © The Royal Society of Chemistry 2022

Published on 09 november 2021. Downloaded on 2025-01-07 13:39:47.

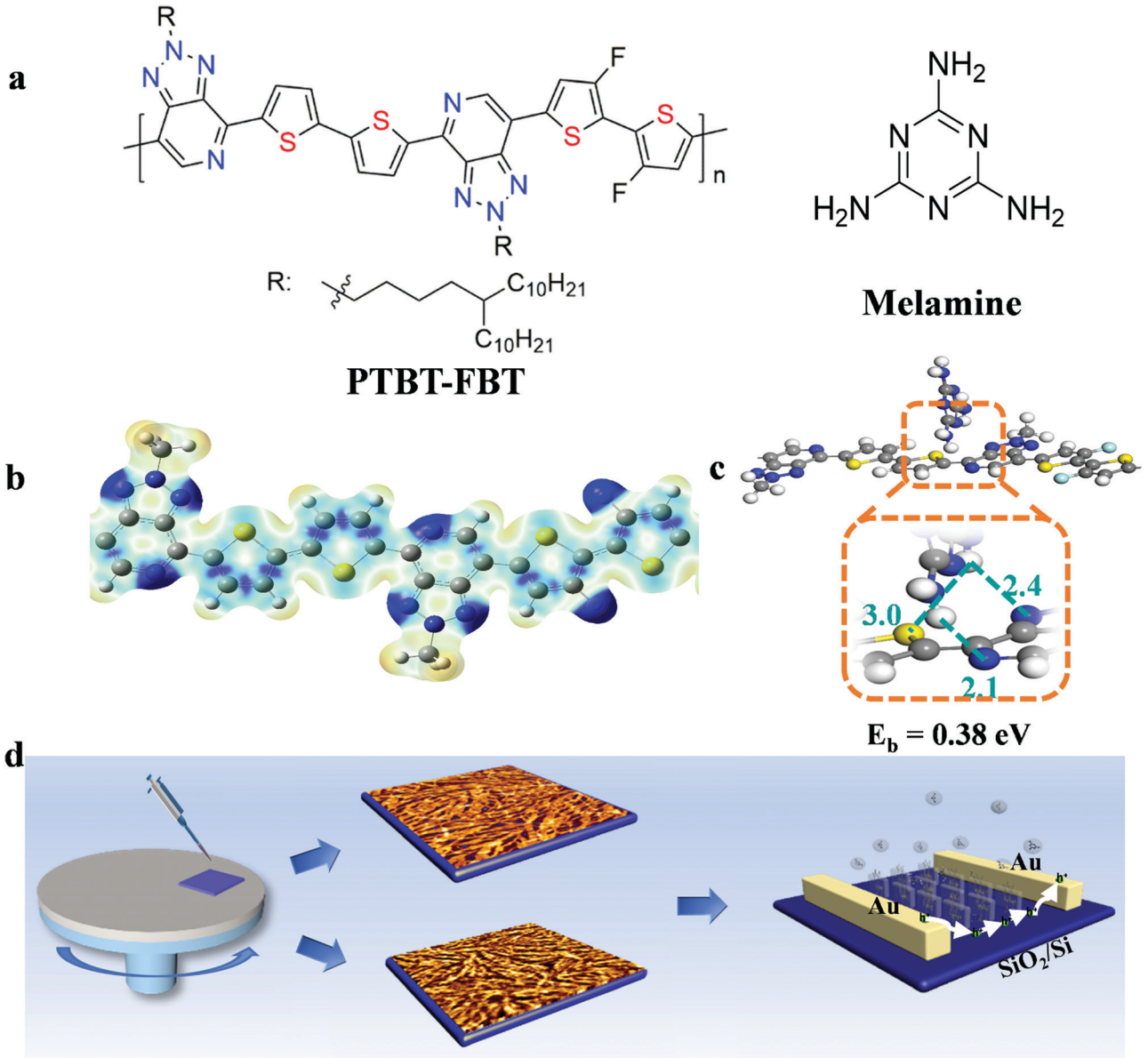

Fig. 1 (a) Chemical structures of PTBT–FBT and melamine. DFT calculations on the adsorption of melamine to the PTBT–FBT polymer. (b) Electrostatic potential map of the PTBT–FBT on an electron density isosurface of 0.08 $Bohr^{-3}$. Blue and red colours represent low and high electrostatic potentials, respectively. (c) Structures and the corresponding binding energies of a melamine molecule adsorbed at the TP position of the PTBT–FBT polymer. (d) Schematic diagram illustrating the preparation of LDPN films and thick films and organic field-effect transistors in contact with melamine.

low-dimensional polymer networks (LDPNs) for the detection of VDAs. To achieve this goal, we designed and synthesized a p-type conjugated polymer PTBT–FBT (in Fig. 1a) with specific functional units containing triazolo[4,5-*c*] pyridine (TP), bithiophene (BT) and 3,3′-difluoro-2,2′-bithiophene (2FBT) to increase the interaction with the solid analytes containing specific groups. Herein, we employed melamine as the targeted solid analyte due to its unique molecular structure with amine groups and inevitable residues in animal feeds.[38] Both the theoretical simulation and experimental results indicated that the absorbed melamine molecules could form intermolecular hydrogen-bonding with PTBT–FBT at the TP position, thereby constraining the transportation of charge carriers, increasing the charge trapping effect and suppressing the output current. Consequently, the sensing resistance of the solid sensors was significantly increased. Compared to conventional analytical instruments including liquid chromatography–mass spectrometry and gas chromatography–triple quadrupole tandem mass spectrometry,[39] the as-prepared PFET-based LDPN sensors exhibited a lower manufacturing cost, a higher detection efficiency and a lower detection limit of below 0.015 ppb (10% changes of resistance) at a low operation voltage of −5 V. The detection limit of the solid sensor was far higher than the international limitation of 2.5 ppm for melamine in animal feeds. Consequently, the strategy proposed here provides a brand-new perspective to prepare high-sensitivity, high-efficiency and

Published on 09 november 2021. Downloaded on 2025-01-07 13:39:47.

low-power-consumption sensing devices for solid detection or biological diagnosis.

Results and discussion

Synthesis and theoretical simulation of PTBT–FBT

A p-type conjugated polymer PTBT–FBT with specific units containing TP, BT and 2FBT (in Fig. 1a) was synthesized. Scheme S1 (ESI†) shows the synthetic route for PTBT–FBT. The detailed synthetic methods are provided in the ESI.† Bromination of commercially available pyridine-3,4-diamine (1) using bromine yielded 2,5-dibromopyridine-3,4-diamine (2). Next, 2 was cyclized with $NaNO_2$ in acetic acid to afford 4,7-dibromo-2*H*-[1,2,3]triazolo [4,5-*c*] pyridine (3). Alkylation of 3 with 1-iodo-5-decylpentadecane gave soluble 4. Regioselective Stille coupling between 4 and 5,5′-bis(trimethylstannyl)-2,2′-bithiophene afforded TP–BT–TP.[40] Stille coupling polymerization reaction between TP–BT–TP and 5,5′-bis(trimethylstannyl)-3,3′-difluoro-2,2′-bithiophene provided the corresponding polymer (PTBT–FBT). The molecular structures of the intermediate products and the monomer were confirmed by NMR tests (Fig. S1–S6, ESI†). The number-average molecular weight (Mn) of PTBT–FBT was determined by high-temperature gel permeation chromatography (GPC) using 1,2,4-tricholorobenzene as the eluent (Fig. S7a, ESI†). PTBT–FBT showed a moderate molecular weight with Mn of 21.0 kDa. Thermogravimetric analysis (TGA) suggested that the polymer displayed good thermal stability with 5% weight loss at a temperature of 400 °C (Fig. S7b, ESI†). The electrochemical behaviour of PTBT–FBT was investigated by cyclic voltammetry (CV) (Fig. S8a, ESI†). The highest occupied molecular orbital (HOMO) and lowest unoccupied molecular orbital (LUMO) energy levels of PTBT–FBT were −5.23 and −3.46 eV, respectively. The UV-vis absorption spectra of PTBT–FBT were tested both in solution and in thin film. PTBT–FBT possessed an optical bandgap of 1.77 eV, which was calculated from the film absorption onset (Fig. S8b, ESI†).

Density functional theory calculations were performed to reveal the adsorption of melamine on the PTBT–FBT polymers. The detailed calculation methods are provided in the ESI.† As shown in the electrostatic potential map of the PTBT–FBT polymer (in Fig. 1b), nitrogen and sulfur atoms of the TP unit together with fluorine and sulfur atoms of the 2FBT unit exhibited higher electronegativities than those of the other atoms. Therefore, these units were possible adsorption sites for the amino groups of melamine molecules. To further verify the adsorption site, the binding energies of a melamine molecule to the TP and BT positions of the PTBT–FBT polymer, referred to as model A for TP–BT and model B for 2FBT, respectively, were calculated using the following equation:

$$E_b = E_{sys} - E_{poly} - E_{mole}$$

where E_{sys}, E_{poly} and E_{mole} represent the total energies of the adsorption system, the polymer and the molecule, respectively. For model A (in Fig. 1c and Table S1, ESI†), it showed that one strong hydrogen bond with a bond length of 2.1 Å between a hydrogen atom of the melamine molecule and a nitrogen atom of the TP unit in the PTBT–FBT polymer is formed. In addition, two extra relatively weak hydrogen bonds between another hydrogen atom of the melamine molecule and one nitrogen and one sulfur atoms of the TP unit in the PTBT–FBT polymer were formed. In comparison, four relatively weak hydrogen bonds were formed in model B between two hydrogen atoms of the melamine molecule, and two fluorine and two sulfur atoms of the BT unit in the PTBT–FBT polymer (in Fig. S9 and Table S2, ESI†). Because of the strong hydrogen bond in model A, the binding energy in this model (0.38 eV) was higher than that of model B (0.25 eV). At room temperature, the adsorption possibility ratio between model A and model B could be estimated to be $e\hat{}(\Delta E/(k_B T)) \approx 154$, where ΔE is the difference in adsorption energy, k_B is the Boltzmann constant and T represents temperature. This result demonstrated that melamine analytes were primarily absorbed on the surface of the polymer film at TP through hydrogen bonding formation. The hydrogen bonding (in Fig. 1c) was formed between the amino groups of melamine molecules and N atoms of TP in the backbone of PTBT–FBT, which served as a conductive bridge to link the amino groups in melamine (as an electron donor) and PTBT–FBT (as an electron acceptor). Our DFT calculations show that the absorption of melamine on PTBT–FBT *via* hydrogen-bonding leads to the increase of the HOMO level, because of the donor effect of the amino groups in melamine (Fig. S10 in the ESI†). Consequently, melamine adsorbed on PTBT–FBT will trap holes in the p-type PTBT–FBT, leading to the increase of the resistance of PTBT–FBT in the presence of melamine. Obviously, introduction of the TP units into the backbone of PTBT–FBT in building up the hydrogen-bonding played a vitally important role.

Fabrication and characterization of LDPNs

The off-center spin-coating strategy was employed to enable the controllable tuning of film thickness and polymer microstructures.[41] As illustrated in Fig. 1d, the octadecyltrichlorosilane (OTS)-treated heavily doped silicon with grown SiO_2 (SiO_2/Si) was placed onto the rotary platform with the largest distance to rotor center of 2.5 cm, followed by the deposition of the PTBT–FBT in *O*-dichlorobenzene solution onto the OTS-treated SiO_2/Si substrate. Next, the polymer film was prepared using an annealing treatment at 150 °C for 10 min. Melamine powders were introduced onto the polymer film to enable effective detection. Since we assumed the importance of LDPNs of PTBT–FBT, variable LDPNs with different film thicknesses were prepared by controlling the concentrations of the polymer solutions using off-center spin-coating. Furthermore, tapping mode atomic force microscopy (AFM) and grazing incident wide-angle X-ray scattering (GIWAXS) were performed to analyze the film morphology, thickness, and molecular packing. Upon decreasing the polymer solution concentration from 5 mg mL^{-1} to 1 mg mL^{-1} (in Fig. 2a), the polymer film thickness was reduced from 24 nm to 6 nm, which satisfied the thickness requirements of low-dimensional films (below 10 nm). Upon

 This journal is © The Royal Society of Chemistry 2022

Published on 09 november 2021. Downloaded on 2025-01-07 13:39:47.

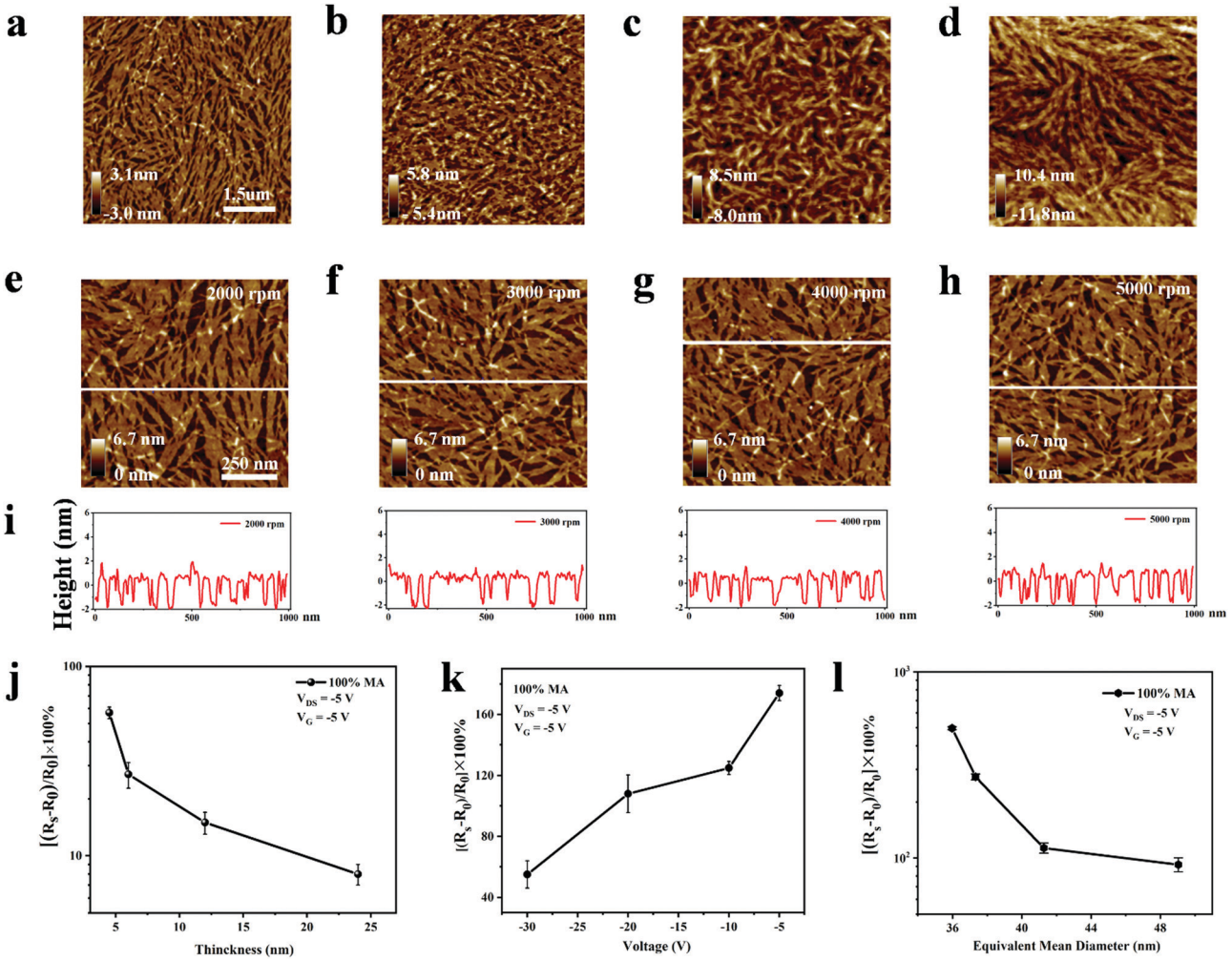

Fig. 2 (a–d) AFM images of thin films at various concentrations (0.7, 1, 3, and 5 mg mL^{-1}) by the off-center at a rotating speed of 5000 rpm. (e–h) AFM images of LDPN films prepared by various off-center spin-coating speeds at a solution concentration of 0.7 mg mL^{-1}. (i) The corresponding height profiles along the indicated lines in (e–h). (j) The sensitivity of the resistance response against the film thickness. (k) The resistance response as a function of equivalent mean diameters. (l) The relationship between the resistance response and operation voltage.

further decreasing the solution concentration to 0.7 mg mL^{-1}, a polymer-film thickness of nearly 3 nm was achieved. The thickness effect on films was certified based on the UV absorption spectra of PTBT–FBT (in Fig. S11a, ESI†). As the film thickness decreased, the signal intensity showed gradual reduction. Furthermore, by reducing the solution concentration from 5 mg mL^{-1} to 0.7 mg mL^{-1}, the size of the crystalline grain gradually decreased and the polymer film was prone to obvious network configurations. Consequently, these results demonstrated that the LDPNs could be fabricated by controlling the solution concentration.

Furthermore, we tuned the LDPN films at a concentration of 0.7 mg mL^{-1} at a spinning speed from 2000 to 5000 rpm. Surprisingly, regardless of the off-center speed, we found that the thicknesses of all the resultant polymer films could remain at a relatively constant value, approximately 3 nm, as estimated from the AFM height images (in Fig. 2). We defined the filling area as a circle and then defined the effective diameter of this cycle as the equivalent mean diameter (EMD) to depict the pore size of the polymer-network films. Fig. 2 also shows the AFM height images of LDPN films prepared subsequently with an increase in the rotation speed (in Fig. S11b and d, ESI†). Specifically, at 2000 rpm, the EMD of the polymer film was the maximum, approximately 49 nm, together with the minimum film coverage onto the Si/SiO_2 substrate of about 66%. Conversely, as the off-center speed increased to 5000 rpm, the polymer film demonstrated the lowest EMD of around 37 nm and the highest coverage of approximately 82%. Therefore, the off-center rotating speed played a crucial role in the microstructure formation (in Table S3, ESI†).

Preparation of highly sensitive PFETs for the detection of VDAs

Using controllable LDPNs, we fabricated FETs with a bottom-contact bottom-gate (BCBG) configuration (see Fig. 1d), which ensures direct contact between the conducting channel and the VDAs. Meanwhile, these devices exhibited typical transfer and output characteristics under the same operation voltages (V_{DS} = −60 V and V_G = −60 V) (in Fig. S12, ESI†). To explore

Published on 09 november 2021. Downloaded on 2025-01-07 13:39:47.

the sensing performance of the solid sensors for melamine detection, the resistance change was defined as the response parameter. It has been universally acknowledged that the charge carrier transport of PFETs primarily occurs in the first few layers of the semiconductor/dielectric interface. To date, there have been no reports on the effective detection of VDAs using conventional PFET-based sensors. This is because the commonly used polymer semiconductor films are generally bulky, which evidently cover the conducting channel and hinder the diffusion of the solid analytes. As shown in Fig. 2, the polymeric film thickness down to the low-dimensional scale structurally resembles networks with the addition of adjustable pore structures. Compared to polymer films featured with multilayer structures, the LDPN films only have a few layers and can, therefore, shorten the migration length of the solid analytes and facilitate their diffusion. In addition, for the polymer we used, it is assumed that the formation of the LDPNs might be attributed to the interaction between molecular chains. A large portion of hydrogen bonding sites are exposed on the surface or near-surface region of the LDPNs, which are favorable for the complete use of the interaction sites and proceeding high-sensing performance. The effects of film thickness on sensing performance were investigated in detail (Fig. 2j). Upon decreasing the polymer film thickness from 24 nm to 3 nm, the change in resistance was considerably enhanced from 8% to 177%, implying that the LDPN film could significantly improve the sensing performance of PFET-based solid sensors.

The pore size is also a vitally important factor that impacts the sensing performance of PFET-based LDPN solid sensors. As shown in Fig. 2k, the resistance response presented a gradually increasing tendency with a decrease in EMD. Thereinto, at the minimum EMD of 35 nm, the resistance response also reached a maximum, approaching 581% (in Fig. S11c, ESI†). In addition, as the size of EMD decreased, the spreading area increased, thereby ensuring the effective contact area between polymer films and melamine powders. Accordingly, the sensing performance of the PFET-based LDPN solid sensors could be considerably enhanced by modulating the pore size of the film.

In order to further explore the detection sensitivity of the solid sensors, the melamine powders were diluted by blending with SiO_2 powders, and subsequently measured using the as-prepared PFET-based LDPN solid sensors. As shown in Fig. S13 (ESI†), most of the sensors exhibited excellent device-to-device uniformity and electrical stability. The electrical stability and the shelf life are a great concern for the application of sensors. We demonstrated the device stability and shelf life by comparing the electrical performance of the sensors stored in a glovebox for 1 day and 7 days. We can observe from Fig. S13a and b (ESI†) that the sensors could be stored within one week with little degradation of electrical performance. It is noteworthy that the solid sensors showed a more significant resistance response at a lower applied voltage (Fig. 2l), which was consistent with the chemical sensor sensing regime based on OFET structures reported.[42–47] Also, a fast response speed below 1.04 s was achieved. In addition, Fig. S14a (ESI†) shows the resistance response of the melamine powders to various melamine concentrations at a gate voltage of −5 V and a source/drain voltage of −5 V. Compared to the distribution of the resistance response for the LDPN solid sensors at each gate voltage, the sensors could exhibit a stable sensing performance at a low gate voltage of −3 V. Fig. 3a shows an obvious linear relationship between the resistance response and the melamine concentration in the analytes at a gate voltage of −3 V, which made the quantitative detection possible for the OFETs at low operation voltage. Under the exposure of pure melamine powders, the resistance change of the solid sensors could reach 177%. With a decrease of the melamine concentration, the resistance change was correspondingly reduced. Moreover, the solid sensors could still exhibit a high resistance response, even at a concentration of as low as 1 ppm.

Because of the amplification of gate effects, the PFETs displayed a very significant resistance increase exceeding 39.6% at a gate voltage of −5 V and a source/drain voltage of −5 V (in Fig. 3b). Therefore, the three-terminal devices demonstrated a 17-times increase in the response to melamine powders compared with the two-terminal devices (in Fig. 3b). In addition, a linear regression equation was established based on the resistance change-concentration linear fitting curves (in Fig. 3a). The limit of detection (calculated using the linear equation in the ESI†) of PFETs (at an operation voltage of −5 V) for melamine powders was 0.015 ppb (based on 10% changes of resistance), which was much lower than the international standards (2.5 ppm). All the above-described results validated that our prepared PFET-based LDPN solid sensors possessed a high sensitivity to melamine. Thus, in this study, we present the first successful fabrication of sensing-performance solid sensors based on LDPN films.

To demonstrate the effect of TP units on the formation of hydrogen bonds with the solid analytes, we fabricated another type of PFET-based solid sensors using PBTTT (in Fig. 3c), respectively. The polymer introduced for comparison was thiophene derivatives, which was distinguishable from PTBT–FBT due to the absence of TP units. Melamine was also used as the target analyte. First, the thick-film (about 30 nm) PFET-based solid sensors were prepared. When the experimental results of both types of PFET-based solid sensors (in Fig. 3d) were compared, we found that the resistance response of PFET with PTBT–FBT was 10-times higher than that of PFET with PBTTT. Next, the PFET-based solid sensors with low-dimensional films (about 7 nm) were also prepared. The comparison results demonstrated that the resistance response of PTBT–FBT was 17-times higher than that of PBTTT (in Fig. 3e). These findings suggested that the introduction of TP units into PTBT–FBT was instrumental for forming hydrogen bonds with the analyte molecules and enhancing the solid detecting sensitivity, which well corresponded with our theoretical simulation results as before. Besides, we compared the resistance response for solid sensors with different film thicknesses based on both types of polymers used. Our findings suggested that decreasing the film thickness to a low-dimensional scale was a universal and significant strategy for realizing effective solid detection based on PFETs.

 This journal is © The Royal Society of Chemistry 2022

Published on 09 november 2021. Downloaded on 2025-01-07 13:39:47.

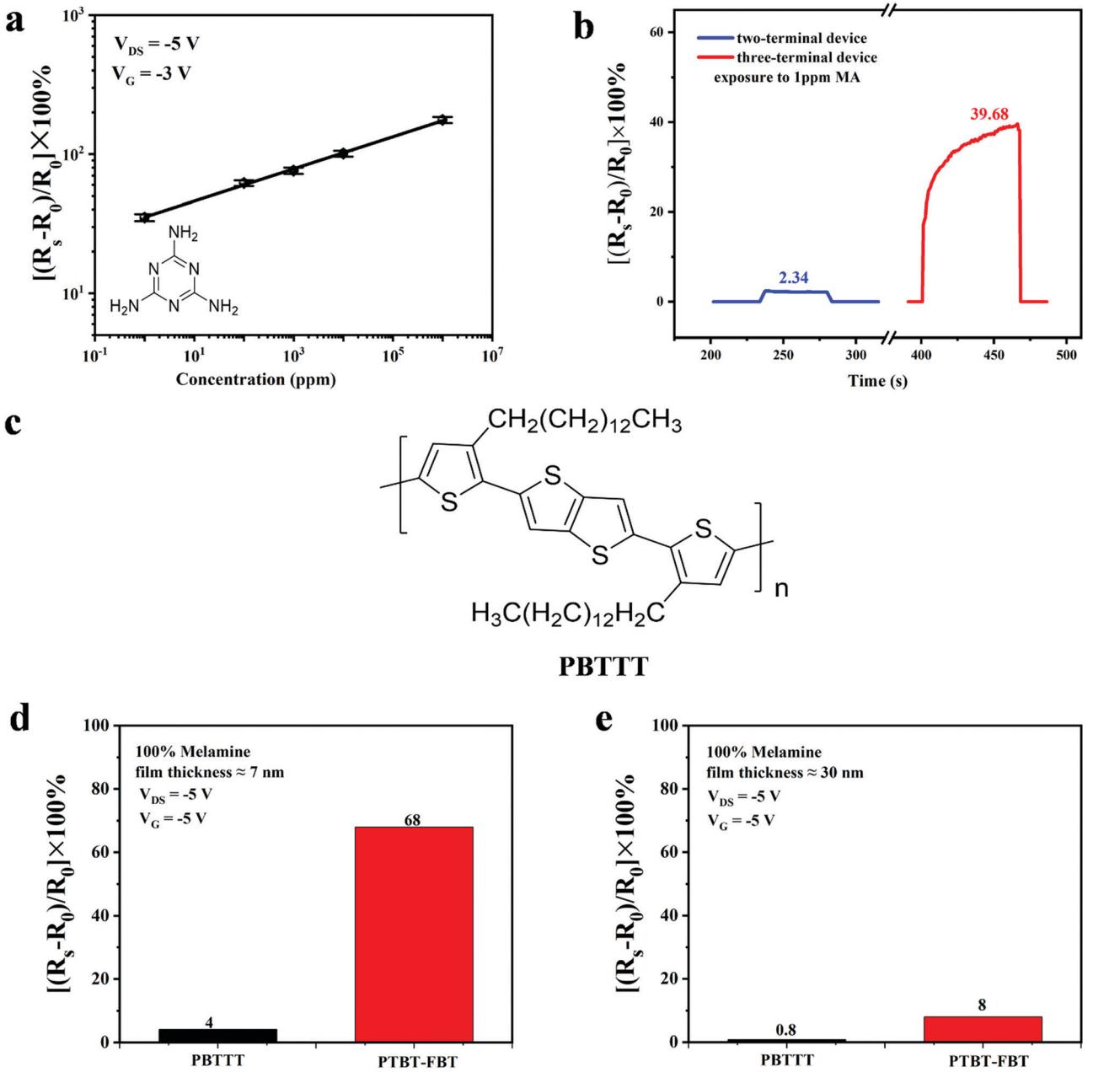

Fig. 3 (a) The sensitivity of resistance response against the concentration of melamine powders. The resistance response of (b) two-terminal and three-terminal devices upon exposure to melamine powders at a concentration of 1 ppm. (c) Chemical structures of PBTTT. Resistance responses of PFET solid sensors based on (d) thick films and (e) LDPN films upon various polymers corresponding to the chemical structures in (c).

To further confirm the influence of hydrogen bonding between solid analytes and PTBT–FBT on the sensing process, we applied the as-prepared LDPN solid sensors to detect other solid chemical analytes, including 1,5-naphthalenediamine ($Naph(NH_3)_2$) and naphthalene (Naph) (the corresponding chemical structures in Fig. S15a, ESI†). For both the analytes, the solid sensors demonstrated the highest response to $Naph(NH_3)_2$, but lowest response to Naph (in Fig. S15b, ESI†). By combining the chemical structures with the resistance change of these analytes, it could be inferred that the response intensity of the solid sensors to chemical analytes may also be dominated by the hydrogen bonding between PTBT–FBT and chemical analytes, as verified by the theoretically calculated results (in Fig. S16, ESI†). It showed that the hydrogen bonding was formed at the absorption position between PTBT–FBT and both chemical analytes (Naph and $Naph(NH_3)_2$). Compared with the adsorption energies of Naph and $Naph(NH_3)_2$ at TP (in Table S1, ESI†) and 2FBT (in Table S2, ESI†) under the same concentration, the corresponding adsorption probability ratio of $Naph(NH_3)_2$ was 7-times and 13-times higher than that of Naph at room temperature, respectively. However, the resistance response of $Naph(NH_3)_2$ was about 11-times higher than

Published on 09 november 2021. Downloaded on 2025-01-07 13:39:47.

that of Naph under the same testing conditions. We propose that the resistance response induced by Naph$(NH_3)_2$ was also caused by the strong hydrogen bonding between Naph$(NH_3)_2$ molecules and PTBT–FBT polymers.

Detection of different VDAs

To validate the versatility of the PFET-based LDPN solid sensors, VDAs with amino groups, including cimaterol and dinitolmide, were employed as the objective analytes. Similar to the dilution process used for melamine, both the VDAs were also mixed and diluted with SiO_2 powders. During the sensing process, the solid sensor was operated under the same bias at various concentrations. As shown from the resistance-change-concentration linear fitting curves in Fig. 4a and b, the resistance response of the solid sensors to both the VDAs were gradually improved with increasing concentration. In order to further verify the resistance response of solid sensors toward VDAs, two types of models for theoretical calculation were also established as described earlier (in Fig. S17, ESI†). It was shown that the absorption sites of both VDAs were TP of PTBT–FBT as well (in Fig. S17 and Tables S1, S3, ESI†). In addition, the hydrogen bonding between the amino groups and nitro groups of the VDA analytes, and the N atoms of TP as well as S atoms of BT in the PTBT–FBT backbone resulted in an effective resistance response. In addition, due to the formation of different-strength hydrogen bonding between VDA analytes and polymer film, the solid sensor showed various response intensities at the same concentration (in Fig. S17f, ESI†), which was beneficial for prescreening different types of VDAs in animal feeds. Consequently, these results demonstrated the importance of hydrogen bonding between polymer and solid analytes during the sensing process. The PFET-based LDPN solid sensors exhibited high sensitivity and high efficiency to detect the existence of VDAs even at a low concentration of 1 ppm.

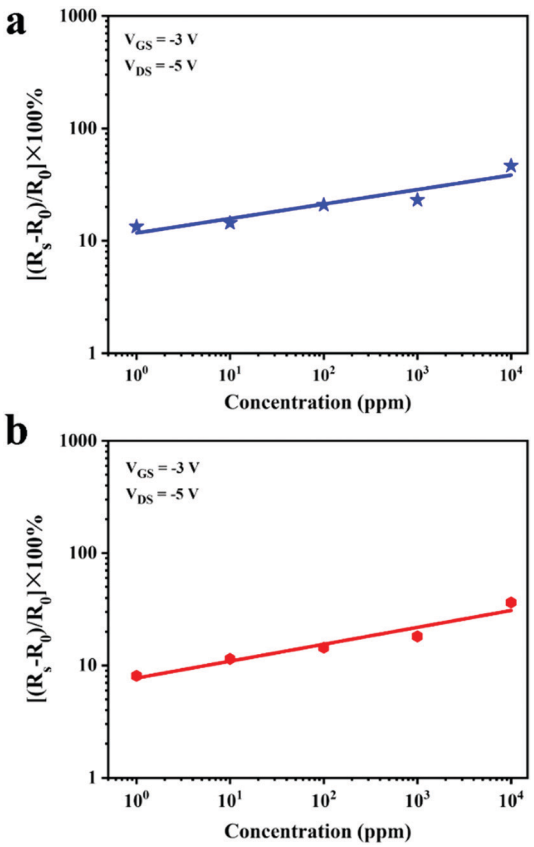

Fig. 4 The sensitivity of the resistance response for various concentrations of (a) cimaterol powders and (b) dinitolmide powders.

Conclusions

A PFET-based LDPN solid sensor was fabricated based on an off-center approach and showed high sensitivity to VDAs. The TP unit in the PTBT–FBT polymer could form intermolecular hydrogen bonding with melamine analytes, thereby improving the capture efficiency. It was further combined with our regulation of LDPNs (nearly 3 nm thickness) to effectively increase the exposure of the conducting channels and the hydrogen bonding sites to confer high sensitivity to the solid analytes. Consequently, the as-fabricated PFET-based LDPN solid sensors could enable a maximum resistance response of 177%, and even retained a desirable response at a melamine concentration of 1 ppm at a low operation voltage below −5 V, which satisfied the requirements of state specified standards for the limited quantity in animal feeds. In addition, the LDPN solid sensors also showed superior versatility for the high-efficiency detection of cimaterol and dinitolmide. These results demonstrated that PFET-based LDPN solid sensors would become a facile and effective candidate for future real-time solid detection or biological diagnosis.

Author contributions

Junhua Kuang conducted the experiments including fabricating sensors and performing the measurements. Junhua Kuang, Kai Liu and Wei Shi organized the paper content. Jie Yang conducted the materials synthesis. Zhiyuan Zhao, Mingchao Shao, Yangshuang Bian, Yanwei Liu, Jinyang Chen and Mingcong Qin provided resources for electrical measurements. Jiechen Dong contributed to the theoretical calculation part. Lang Jiang, Yunlong Guo and Yunqi Liu supervised the work by giving the idea, designing the experiments, and explaining the experimental results.

Conflicts of interest

There are no conflicts to declare.

Acknowledgements

This work is supported by grants from the National Key R&D Program of China (grant no. 2018YFA0703200), the National Natural Science Foundation of China (No. 21922511, 91833304, 91833306, 61890940, 21633012 and 51873216), the Strategic Priority Research Program of the Chinese Academy of Sciences

 This journal is © The Royal Society of Chemistry 2022

Published on 09 november 2021. Downloaded on 2025-01-07 13:39:47.

(No. XDB30000000), and the CAS Key Research Program of Frontier Sciences (grant no. QYZDY-SSW-SLH029).

References

1 A. C. Valese, L. Molognoni, N. C. de Souza, L. A. de Sa Ploencio, A. C. O. Costa, F. Barreto and H. Daguer, *J. Chromatogr. B: Anal. Technol. Biomed. Life Sci.*, 2017, **1053**, 48–59.
2 S. Wang, H. Y. Zhang, L. Wang, Z. J. Duan and I. Kennedy, *Food Addit. Contam.*, 2006, **23**, 362–384.
3 L. Torsi, G. M. Farinola, F. Marinelli, M. C. Tanese, O. H. Omar, L. Valli, F. Babudri, F. Palmisano, P. G. Zambonin and F. Naso, *Nat. Mater.*, 2008, **7**, 412–417.
4 M. Y. Lee, H. R. Lee, C. H. Park, S. G. Han and J. H. Oh, *Acc. Chem. Res.*, 2018, **51**, 2829–2838.
5 X. Wu, S. Mao, J. Chen and J. Huang, *Adv. Mater.*, 2018, **30**, 1705642.
6 H. Li, W. Shi, J. Song, H. J. Jang, J. Dailey, J. Yu and H. E. Katz, *Chem. Rev.*, 2019, **119**, 3–35.
7 W. Huang, K. Besar, R. LeCover, A. M. Rule, P. N. Breysse and H. E. Katz, *J. Am. Chem. Soc.*, 2012, **134**, 14650–14653.
8 Y. Zang, F. Zhang, D. Huang, C. A. Di, Q. Meng, X. Gao and D. Zhu, *Adv. Mater.*, 2014, **26**, 2862–2867.
9 B. Peng, S. Huang, Z. Zhou and P. K. L. Chan, *Adv. Funct. Mater.*, 2017, **27**, 1700999.
10 A. S. Sizov, A. A. Trul, V. Chekusova, O. V. Borshchev, A. A. Vasiliev, E. V. Agina and S. A. Ponomarenko, *ACS Appl. Mater. Interfaces*, 2018, **10**, 43831–43841.
11 J. H. Lee, Y. Seo, Y. D. Park, J. E. Anthony, D. H. Kwak, J. A. Lim, S. Ko, H. W. Jang, K. Cho and W. H. Lee, *Sci. Rep.*, 2019, **9**, 21.
12 S. Zhang, Y. Zhao, X. Du, Y. Chu, S. Zhang and J. Huang, *Small*, 2019, **15**, 1805196.
13 H. Li, Y. Shi, G. Han, J. Liu, J. Zhang, C. Li, J. Liu, Y. Yi, T. Li, X. Gao, C. Di, J. Huang, Y. Che, D. Wang, W. Hu, Y. Liu and L. Jiang, *Angew. Chem., Int. Ed.*, 2020, **59**, 4380–4384.
14 P. K. Sahu, R. K. Pandey, R. Dwivedi, V. N. Mishra and R. Pra-kash, *Sci. Rep.*, 2020, **10**, 2981.
15 S. Yuvaraja, S. G. Surya, V. Chernikova, M. T. Vijjapu, O. Shekhah, P. M. Bhatt, S. Chandra, M. Eddaoudi and K. N. Salama, *ACS Appl. Mater. Interfaces*, 2020, **12**, 18748–18760.
16 S. C. Mannsfeld, B. C. Tee, R. M. Stoltenberg, C. V. Chen, S. Barman, B. V. Muir, A. N. Sokolov, C. Reese and Z. Bao, *Nat. Mater.*, 2010, **9**, 859–864.
17 Y. Li, S. Luo, M.-C. Yang, R. Liang and C. Zeng, *Adv. Funct. Mater.*, 2016, **26**, 2900–2908.
18 Z. Wang, S. Guo, H. Li, B. Wang, Y. Sun, Z. Xu, X. Chen, K. Wu, X. Zhang, F. Xing, L. Li and W. Hu, *Adv. Mater.*, 2019, **31**, 1805630.
19 L. Li, J. Zheng, J. Chen, Z. Luo, Y. Su, W. Tang, X. Gao, Y. Li, C. Cao, Q. Liu, X. Kang, L. Wang and H. Li, *Adv. Mater. Interfaces*, 2020, **7**, 2000743.
20 M. El Gemayel, M. Treier, C. Musumeci, C. Li, K. Mullen and P. Samori, *J. Am. Chem. Soc.*, 2012, **134**, 2429–2433.
21 C. Wang, X. Ren, C. Xu, B. Fu, R. Wang, X. Zhang, R. Li, H. Li, H. Dong, Y. Zhen, S. Lei, L. Jiang and W. Hu, *Adv. Mater.*, 2018, **30**, 1706260.
22 Y. Yao, L. Zhang, T. Leydecker and P. Samori, *J. Am. Chem. Soc.*, 2018, **140**, 6984–6990.
23 Q. Li, Y. Guo and Y. Liu, *Chem. Mater.*, 2019, **31**, 6359–6379.
24 M. A. Iqbal, A. Liaqat, S. Hussain, X. Wang, M. Tahir, Z. Urooj and L. Xie, *Adv. Mater.*, 2020, **32**, 2002628.
25 J. Liu, L. Jiang, J. Shi, C. Li, Y. Shi, J. Tan, H. Li, H. Jiang, Y. Hu, X. Liu, J. Yu, Z. Wei, L. Jiang and W. Hu, *Adv. Mater.*, 2020, **32**, 1906122.
26 A. Wadsworth, Z. Hamid, J. Kosco, N. Gasparini and I. McCul-loch, *Adv. Mater.*, 2020, **32**, 2001763.
27 O. Knopfmacher, M. L. Hammock, A. L. Appleton, G. Schwartz, J. Mei, T. Lei, J. Pei and Z. Bao, *Nat. Commun.*, 2014, **5**, 2954.
28 M. Y. Lee, H. J. Kim, G. Y. Jung, A. R. Han, S. K. Kwak, B. J. Kim and J. H. Oh, *Adv. Mater.*, 2015, **27**, 1540–1546.
29 R. H. Tian, S. Regonda, S. Greene, G. Zhi, J. H. Ding and W. Hu, *IEEE Sens. J.*, 2013, 1819–1822.
30 J. Huang, G. Zhang, X. Zhao, X. Wu, D. Liu, Y. Chu and H. E. Katz, *J. Am. Chem. Soc.*, 2017, **139**, 12366–12369.
31 X. Guo, A. Facchetti and T. J. Marks, *Chem. Rev.*, 2014, **114**, 8943–9021.
32 Y. H. Lee, M. Jang, M. Y. Lee, O. Y. Kweon and J. H. Oh, *Chem*, 2017, **3**, 724–763.
33 M. Li, D. K. Mangalore, J. Zhao, J. H. Carpenter, H. Yan, H. Ade, H. Yan, K. Mullen, P. W. M. Blom, W. Pisula, D. M. de Leeuw and K. Asadi, *Nat. Commun.*, 2018, **9**, 451.
34 A. F. Paterson, S. Singh, K. J. Fallon, T. Hodsden, Y. Han, B. C. Schroeder, H. Bronstein, M. Heeney, I. McCulloch and T. D. Anthopoulos, *Adv. Mater.*, 2018, **30**, 1801079.
35 J. Yang, Z. Zhao, S. Wang, Y. Guo and Y. Liu, *Chem*, 2018, **4**, 2748–2785.
36 Z. F. Yao, Y. Q. Zheng, Q. Y. Li, T. Lei, S. Zhang, L. Zou, H. Y. Liu, J. H. Dou, Y. Lu, J. Y. Wang, X. Gu and J. Pei, *Adv. Mater.*, 2019, **31**, 1806747.
37 M. Li, H. Bin, X. Jiao, M. M. Wienk, H. Yan and R. A. J. Janssen, *Angew. Chem., Int. Ed.*, 2020, **59**, 846–852.
38 R. P. Dalal and D. S. Goldfarb, *Nat. Rev. Nephrol.*, 2011, **7**, 267–274.
39 A. Kumar, A. Bhattacharyya, R. Shinde, M. Dhanshetty, C. T. Elliott and K. Banerjee, *J. Chromatogr. A*, 2020, **1627**, 461416.
40 L. Ying, F. Huang and G. C. Bazan, *Nat. Commun.*, 2017, **8**, 14047.
41 Y. Yuan, G. Giri, A. L. Ayzner, A. P. Zoombelt, S. C. Mannsfeld, J. Chen, D. Nordlund, M. F. Toney, J. Huang and Z. Bao, *Nat. Commun.*, 2014, **5**, 3005.
42 J. Huang, J. Sun and H. E. Katz, *Adv. Mater.*, 2008, **20**, 2567.
43 J. Huang, J. Miragliotta, A. Becknell and H. E. Katz, *J. Am. Chem. Soc.*, 2007, **129**, 9366.
44 J. Huang, T. J. Dawidczyk, B. J. Jung, J. Sun, A. F. Mason and H. E. Katz, *J. Mater. Chem.*, 2010, **20**, 2644.
45 B. J. Jung, K. Lee, J. Sun, A. G. Andreou and H. E. Katz, *Adv. Funct. Mater.*, 2010, **20**, 2930.
46 M. Mushrush, A. Facchetti, M. Lefenfeld, H. E. Katz and T. J. Marks, *J. Am. Chem. Soc.*, 2003, **125**, 9414.
47 T. Yamamoto and K. Takimiya, *J. Am. Chem. Soc.*, 2007, **129**, 2224.